

Geomaterials (Sedimentology)

Sedimentology and chemostratigraphy of the Bwipe Neoproterozoic cap dolostones (Ghana, Volta Basin): A record of microbial activity in a peritidal environment

Anne Nédélec^{a,*}, Pascal Affaton^b, Christian France-Lanord^c,
André Charrière^a, Javier Alvaro^d

^a UMR 5563–LMTG, université Paul-Sabatier, 14, avenue Édouard-Belin, 31400 Toulouse, France

^b UMR 6635–CEREGE, Europôle méditerranéen de l'Arbois, BP 80, 13545 Aix-en-Provence cedex 04, France

^c UPR 2300–CRPG, 15, rue Notre-Dame-des-Pauvres, 54501 Vandœuvre-lès-Nancy, France

^d UMR 801–LP3, UFR Sciences de la Terre, université Lille-1, bâtiment SN5, 59655 Villeneuve-d'Ascq cedex, France

Received 15 November 2004; accepted 26 May 2005

Available online 10 August 2005

Written on invitation of the Editorial Board.

Abstract

Neoproterozoic glacial and post-glacial sediments from the Volta Basin (West Africa) form a stratigraphic ‘Triad’ of tillites, carbonates and cherts. The carbonates that cap the tillites were studied in detail at Bwipe (Ghana), in the western part of the basin. They are made of finely-laminated dolostones with well-preserved sedimentary features, suggesting that dolomite formation was pencontemporaneous of deposition in a warm, arid peritidal environment, with microbial activity. Rare-earth element distribution display seawater-like patterns. Redox-sensitive trace elements indicate suboxic conditions. High Ba/Al ratios can be related to high organic productivity. $\delta^{13}\text{C}$ values are nearly constant at -3.7‰ and $\delta^{18}\text{O}_{\text{PDB}}$ are about -6‰ . $^{87}\text{Sr}/^{86}\text{Sr}$ ratios range between 0.7061 and 0.7073. The $\delta^{13}\text{C}$ signatures are nearly similar to those of coeval cap dolostones from the northern part of the Basin. The dolostones change upwards to limestones with secondary textures, as well as more negative $\delta^{13}\text{C}$ and higher $^{87}\text{Sr}/^{86}\text{Sr}$ ratio. Therefore, only the dolostones witness the post-glacial conditions in seawater. It is proposed that, due to a bloom of microbial productivity following ice thaw, organic matter likely accumulated at the water–sediment interface and was consumed by sulphate-reducing bacteria, leading to the precipitation of $\delta^{13}\text{C}$ -negative dolomite. This microbially mediated model is supported by present-day field evidence from hypersaline lagoons in Brazil and by previously published culture experiments. It is consistent with the sedimentological and geochemical data from the Ghana cap dolostones and can be applied to other Neoproterozoic cap dolostones worldwide. *To cite this article: A. Nédélec et al., C. R. Geoscience 339 (2006).*

© 2006 Académie des sciences. Published by Elsevier Masson SAS. All rights reserved.

Résumé

Sédimentologie et chimostratigraphie des cap dolomies néoproterozoïques de Bwipe (Ghana, Bassin des Volta) : un témoin de l'activité microbienne dans un environnement péritidal. Les sédiments glaciaires et post-glaciaires du bassin des Volta (Afrique occidentale) constituent une Triade formée de tillites, carbonates et silicites. Les *cap carbonates* qui surmontent directement les tillites ont été étudiés en détail à Bwipe (Ghana), dans l'Ouest du bassin. Ce sont des dolomies finement laminées

* Corresponding author.

E-mail address: nedelec@lmtg.obs-mip.fr (A. Nédélec).

ayant conservé des caractères sédimentaires primaires, indiquant que la formation de la dolomie est pénécemporaine du dépôt et s'est produite en conditions péritidales, sous un climat chaud et aride et en présence d'activité microbienne. Les spectres de terres rares sont de type eau de mer. Les teneurs en éléments traces sensibles aux conditions rédox indiquent des conditions suboxiques. La valeur élevée de Ba/Al suggère une productivité élevée. $\delta^{13}\text{C}$ reste à peu près constant à -3.7% . $\delta^{18}\text{O}_{\text{PDB}}$ est voisin de -6% . $^{87}\text{Sr}/^{86}\text{Sr}$ varie entre 0,7061 et 0,7073. La signature isotopique en carbone est très voisine de celle des *cap dolomies* du Nord du bassin. Vers le haut de la série, les dolomies sont remplacées par des calcaires présentant des recristallisations secondaires, des valeurs plus négatives de $\delta^{13}\text{C}$ et une augmentation de $^{87}\text{Sr}/^{86}\text{Sr}$. Ces signatures isotopiques sont donc considérées comme secondaires. Seules les dolomies de base, non modifiées, sont représentatives des conditions marines post-glaciaires. On propose que, consécutivement à une explosion de productivité microbienne à la fonte des glaces, la matière organique se soit accumulée à l'interface eau-sédiment. La dégradation de la matière organique par des bactéries sulfato-réductrices en conditions anoxiques conduit alors à la précipitation de dolomite appauvrie en ^{13}C . Ce modèle organogénétique s'appuie sur un analogue actuel observé dans des lagunes hypersalées du Brésil et sur des résultats expérimentaux déjà publiés. Il rend compte des données sédimentologiques et géochimiques observées dans les *cap dolomies* du Ghana et peut s'appliquer à d'autres *cap dolomies* néoprotozoïques ailleurs dans le monde. **Pour citer cet article :** A. Nédélec et al., C. R. Geoscience 339 (2006).

© 2006 Académie des sciences. Published by Elsevier Masson SAS. All rights reserved.

Keywords: Neoproterozoic; Dolostone; C Isotopes; Peritidal environment; Sulphate-reducing bacteria; Ghana

Mots clés : Néoprotozoïque ; Dolomie ; Isotopes de C ; Environnement péritidal ; Bactéries sulfato-réductrices ; Ghana

Version française abrégée

Introduction et contexte géologique

Les dépôts glaciaires néoprotozoïques, dus à des glaciations quasi-globales [25], sont surmontés de *cap carbonates* peu épais, qui sont caractérisés par une valeur négative de $\delta^{13}\text{C}$ [15]. Nous présentons une étude sédimentologique et géochimique détaillée des *cap carbonates* qui affleurent au Ghana, dans l'Ouest du bassin des Volta (Fig. 1). Ces carbonates forment la base du supergroupe de la Pendjari et correspondent à une série marine transgressive [1]. À l'est du Bassin, la datation des nappes d'avant-pays de la chaîne panafricaine [4] fournit un âge minimal de 620 Ma pour les *cap carbonates*.

Sédimentologie

Les carbonates de Bwipe commencent par une dizaine de mètres de dolomies (*cap carbonates* sensu stricto), reposant directement sur les tillites. Vers le haut, les dolomies passent à des calcaires, avec des intercalations d'argiles et de silexites. Les dolomies présentent des caractères primaires très bien préservés, contrairement aux calcaires (Fig. 2b et c). On peut y distinguer trois groupes (Fig. 1d et Tableau 1) :

- la partie inférieure (échantillons 7099 à 7109) comprend deux microfaciès. Le microfaciès A présente des lamines dolomicritiques régulières peltoïdales où un pseudomorphe de filament bactérien a été observé (Fig. 2d). Le microfaciès B, de plus forte énergie,

correspond à des lamines irrégulières litharénitiques (Fig. 2e–h). L'alternance de ces deux microfaciès indique des conditions hydrodynamiques changeantes, avec apports terrigènes épisodiques ;

- la partie moyenne (échantillons 7112 à 7146) est formée de laminites régulières et homogènes, constituées de micrite peltoïdale (microfaciès A: Fig. 3a). Des *bird eyes* planaires dénotent le développement d'un tapis microbien gênant les dégagements gazeux produits par la dégradation de matière organique (Fig. 3b). Localement, on observe des pseudomorphes de cristaux de gypse. Le milieu de dépôt correspond alors à une vase stable et protégée ;
- la partie supérieure riche en lamines microbiennes d'allure ondulée montre l'installation d'un tapis stromatolitique.

Ces différents caractères indiquent un environnement péritidal [3] (terme regroupant la zone subtidale temporairement émergée, la zone intertidale et la zone supratidale épisodiquement ennoyée) sous un climat chaud et aride [35].

Chimiostratigraphie

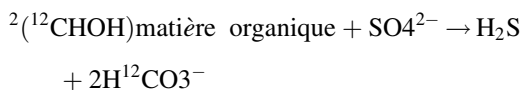
Les compositions chimiques des carbonates de Bwipe sont données dans le Tableau 2. La distribution verticale des éléments majeurs est présentée sur la Fig. 4 et celle des éléments traces sur la Fig. 5. On note la teneur élevée des carbonates en manganèse (Fig. 2h). Les éléments chalcophiles sensibles aux conditions rédox permettent d'estimer le degré d'oxydation lors du dépôt [38]. On constate que les teneurs normalisées à Al

dépassent largement les teneurs moyennes des shales. L'enrichissement relatif en As, Cd et Mo à certains niveaux indique des conditions suboxiques. La présence de Cd est un très bon indicateur de sulfato-réduction [7]. Le rapport $V/(V + Ni)$ [13,27,37] indique des conditions oxiques à dysoxiques. Le rapport Ba/Al (Fig. 6b) témoigne d'une productivité primaire élevée [8,9]. Les spectres de terres rares normalisés aux shales australiens post-archéens sont de type eau de mer ([11]; Fig. 7). Ils présentent une anomalie négative en Ce très faible, indiquant des conditions suboxiques [49].

Les valeurs de $\delta^{13}C$ demeurent à peu près constantes et voisines de $-3,7\%$ (Fig. 8), soit des valeurs légèrement plus faibles, mais comparables à celles obtenues au nord du bassin [34]. On en déduit que ces valeurs ont une signification au moins régionale, sinon globale [15]. Toutefois, seule la signature isotopique des dolomies est prise en considération, mais pas celle des calcaires où les caractères sédimentologiques initiaux n'ont pas été préservés. Les rapports $^{87}Sr/^{86}Sr$ obtenus après dissolution ménagée dans l'acide acétique (pour éviter la contamination par du Sr radiogénique) correspondent à des valeurs faibles (0,7061–0,7073). Reportées dans la courbe d'évolution isotopique du Sr (Fig. 9; [5,30]), ces valeurs sont compatibles avec un âge post-Marinoen (630 Ma) ou même post-Sturtien (730–680 Ma) pour le dépôt de ces *cap carbonates*.

Interprétation et conclusion : un modèle organogénétique pour la formation des cap dolomies

La précipitation inorganique de la dolomite pose problème, même dans de l'eau de mer sursaturée en carbonates [46]. Toutefois, la dolomite des *cap carbonates* de Bwipe semble bien précoce, pénécotemporaine du dépôt. Par ailleurs, ces roches montrent des signes d'activité organique importante en conditions suboxiques. Dans ces conditions, la matière organique est dégradée par les bactéries sulfato-réductrices qui produisent des ions bicarbonates enrichis en ^{12}C :



En consommant le sulfate, cette réaction détruit le lien entre magnésium et sulfate, qui constitue un puissant inhibiteur de la formation de dolomite. Celle-ci peut alors précipiter et sa signature isotopique négative en C indique la contribution des bicarbonates formés par la réaction ci-dessus (Fig. 9). Ce processus a été observé dans les conditions récentes et actuelles [29,42]

et reproduit en culture [41,47]. Il a pu jouer un rôle primordial dans les zones péritidales protégées lors des déglaciations néoprotozoïques. En effet, le passage rapide d'un climat froid à un climat chaud a induit la réactivation de la circulation océanique et celle du cycle hydrologique, d'où des apports nutritifs considérables à l'océan, permettant probablement une formidable floraison microbienne [26]. Les possibilités de reminéralisation complète de la matière organique étant alors dépassées, les bactéries sulfato-réductrices entrent en jeu et laissent leur marque dans la signature isotopique caractéristique des *cap dolomies*.

1. Introduction

Cap carbonates are ubiquitous deposits that formed just after the unusually severe Neoproterozoic ice ages, giving birth to the Snowball-Earth hypothesis [25]. Despite their reduced thickness (usually 5–10 m for the cap dolostones), their very peculiar geochemical features raised a lot of interest, but their conditions of formation are still poorly known. Most published works deal with carbon isotope signatures that are typically negative [15]. Lithological characterization is sometimes provided [21], as well as other stable isotope data (O, Sr, S), but major and trace element contents are rarely analysed. Our aim is to get a complete sedimentological and geochemical characterization of Neoproterozoic post-glacial cap carbonates from the western part of the Volta Basin in Ghana (Fig. 1a). C and O isotope compositions of similar rocks from the northern part of the Volta Basin were already provided by Porter et al. [34]. Our new data set offers the opportunity for basin scale correlation and for discussion of the origin of cap carbonates.

2. Geological setting

The Volta Basin comprises Meso- and Neoproterozoic to Lower Palaeozoic sediments deposited on the Eburnean (2.1 Ga or older) basement of the Man Shield, that have been described in detail by Affaton [1]. Sedimentation was first terrigenous and epicontinental (Bombouaka Supergroup), then marine in the form of a passive margin sequence (Pendjari Supergroup) followed by the molassic foreland deposits of the Tamale Supergroup (Fig. 1b). Conglomerates at the base of the Tamale Supergroup display an angular unconformity with respect to the underlying Pendjari Supergroup, a consequence of the formation of the nearby Dahomeyide belt [2], the southern extension of the Pan-African Trans-Saharan belt in Hoggar (Fig. 1a). The

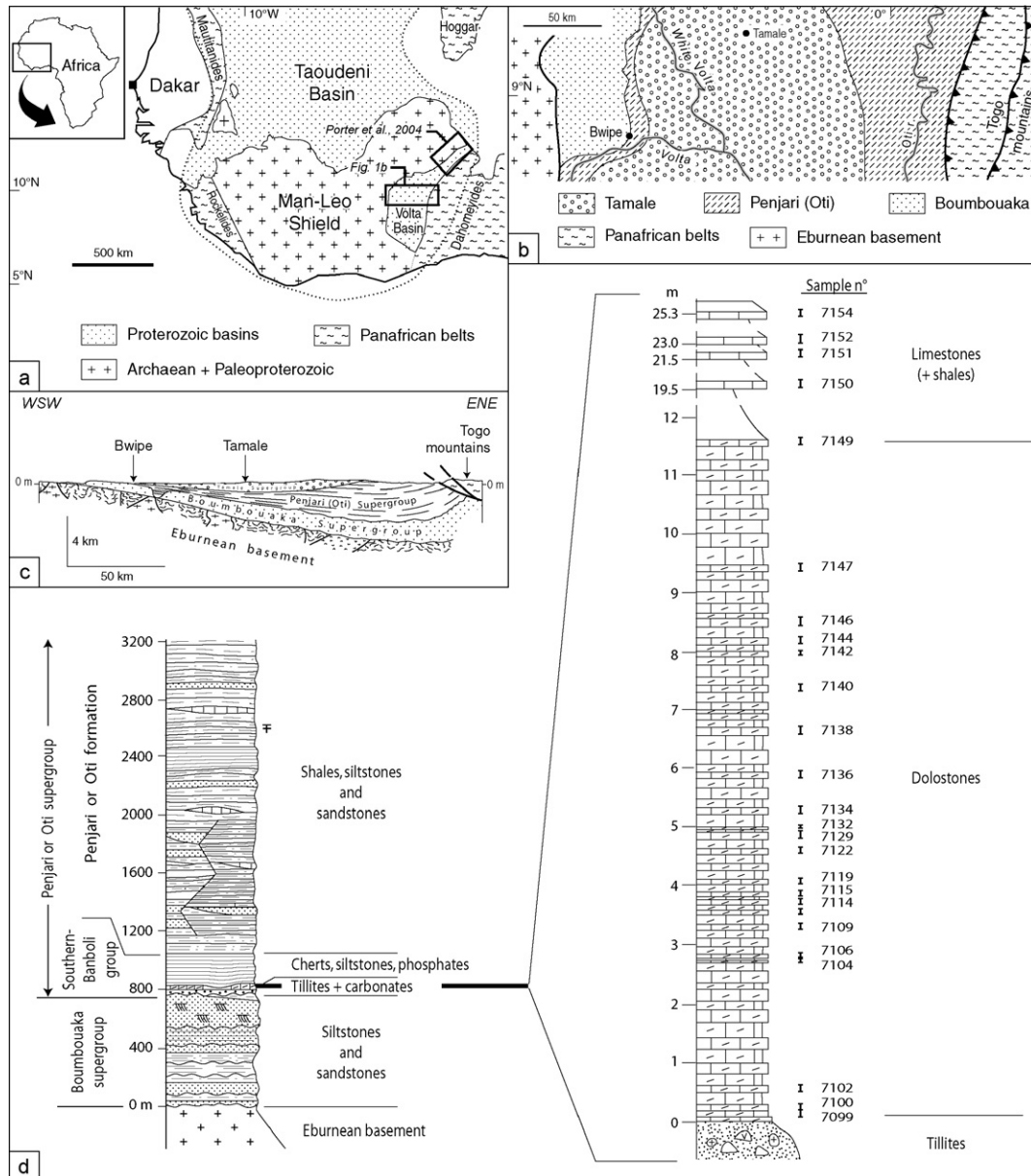


Fig. 1. (a) Location of the Volta Basin in the West Africa craton. (b) Geological map of the studied area. (c) Cross-section of the Volta Basin. (d) Stratigraphy of the Proterozoic in the Bwipé area; (b, c) redrawn from [1].

Fig. 1. (a) Situation du bassin des Volta dans le craton Ouest-Africain. (b) Carte géologique du secteur d'étude. (c) Coupe du bassin des Volta. (d) Stratigraphie du Protérozoïque dans la région de Bwipé ; (b, c) redessinés d'après [1].

Pan-African orogeny along the eastern border of the West African craton resulted from oceanic closure and continent–continent collision with the poorly known Saharan craton and was recently dated at about 620 Ma [20]. This orogeny was responsible for folds and thrusts in the eastern part of the Boumbouaka and Penjari Supergroups (Fig. 1c), but the sediments in the Volta Basin experienced no metamorphism. A muscovite Ar/Ar age of 608 (± 1) Ma was obtained from the external

nappe of the Togo mountains ([4]; Fig. 1b and c). Therefore, an age older than 620 Ma is proposed for the Penjari Supergroup, consistent with a Marinoan (ca 635 Ma) or Sturtian (ca 700 Ma) age for the glaciogenic deposits.

The base of the Penjari Supergroup consists of a stratigraphic 'Triad' made of tillites, carbonates and bedded cherts (actually silicified shales) in this stratigraphic order (Fig. 1d). The Triad has been

recognized along the western part of the Basin in Ghana, as well as further north in northern Togo and southern Burkina Faso, where striated pavements demonstrate the glacial origin of the tillites [34]. Cap carbonates overlying discontinuous outcrops of tillites were sampled in Ghana near Bwipe (Fig. 1b, c), where the carbonate thickness (25 m) is greater than to the north (maximum thickness: 2.40 m in Arli, Burkina Faso). The stratigraphic section at Bwipe is provided in Fig. 1d.

3. Sedimentology

3.1. Microfacies

Tillites are directly overlain by a carbonate formation, whose first 12 metres are made of finely laminated dolostones, which constitute the ‘cap carbonates’ sensu stricto. These rocks are especially well-preserved, fenestral, peloidal and microbial dolostones, with a millimetre-scale lamination, sometimes accompanied by colour changes from yellowish to light pink (Fig. 2a). Up section, the carbonate rocks are limestones, where secondary phenomena have erased any primary sedimentary features (Fig. 2b and c). Therefore, our study is mainly focussed on the better preserved dolostones. Twenty-five carbonate samples have been collected and their position in the section is indicated in Fig. 1d. Microfacies and related structures are presented in Table 1. The cap dolostones can be divided in three parts:

– The lower part (samples 7099 to 7109) is made of heterogeneous wackestones to packstones with millimetre- to centimetre-thick alternation of two microfacies (A and B), made of clean and litharenitic dolostones respectively. Microfacies A of lower energy is characterized by roughly parallel regular laminations formed by peloidal, sometimes vuggy, dolomicrite. A pseudomorph of microbial filament can be recognized in one peloid (Fig. 2d). Microfacies B of relatively higher energy displays irregular laminations, locally eroded by microchannel infills, and contains exogeneous lithoclasts (e.g., a small pebble of garnet micaschist: Fig. 1e and f), detrital quartz and feldspar, as well as micritic intraclasts. Such alternating microfacies provide evidence for changing hydrodynamic conditions corresponding to episodic terrigenous inputs. Microstalactites formed in some lamina-parallel open spaces or cracks (Fig. 2e), indicating periodic aerial exposures of the wet sediment.

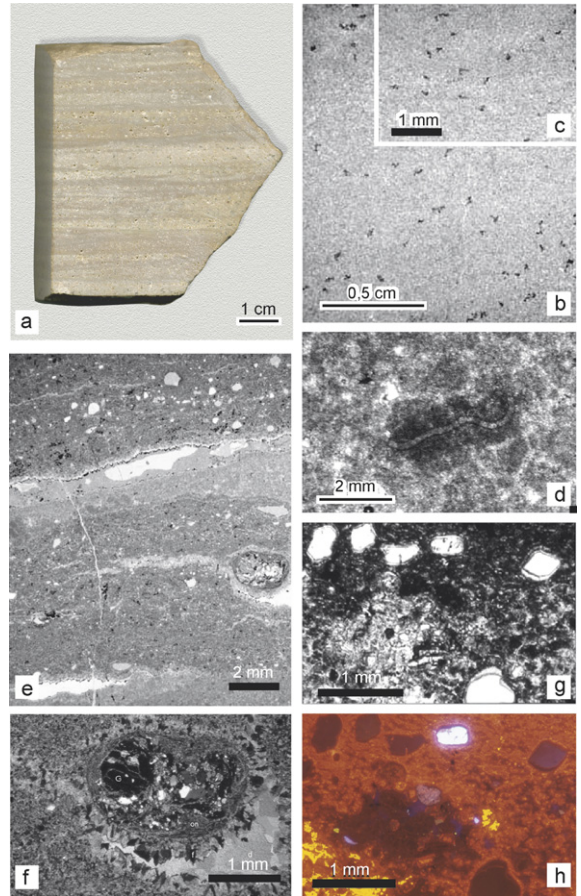


Fig. 2. (a) Dolomite sample 7146. (b, c) Details of recrystallized limestone 7150. (d) Pseudomorph of microbial filament within a peloid (dolomite 7109). (e) Sedimentary sequences of dolomite 7109 with litharenitic laminae (microfacies B); microstalactites underline the top of a small cavity. (f) Detail under crossed polars: a small garnet-micaschist pebble with underlying fenestral porosity infilled by fibrous and drusy carbonate cements. (g) Detail of a sandy lamina displaying the fine cement surrounding the grains. (h) Idem under cathodoluminescence.

Fig. 2. (a) Dolomie 7146. (b, c) Détails du calcaire recristallisé 7150. (d) Pseudomorphe de filament microbien dans un pelétoïde de la dolomie 7109. (e) Séquences sédimentaires dans la dolomie 7109 avec lamines litharénitiques (microfacies B); des microstalactites bordent le plafond d'une petite cavité. (f) Détail en lumière polarisée et analysée d'un microgalet de micaschiste à grenat et de la porosité fenestrale en dessous avec un remplissage de carbonate fibreux et drusifforme. (g) Détail d'une lamine sableuse montrant une fine couche de ciment autour des grains. (h) Idem en cathodoluminescence.

– The middle part (samples 7112 to 7146) comprises homogeneous, regular laminites (microfacies A). Distinct light-dark (< 1-mm-thick) microlaminae occur, locally defined by thin (50–200 μm) gently curved dolomicritic layers (Fig. 3a). Extraclasts are generally lacking. From bottom to top, the laminae thicken and their boundaries become more diffuse.

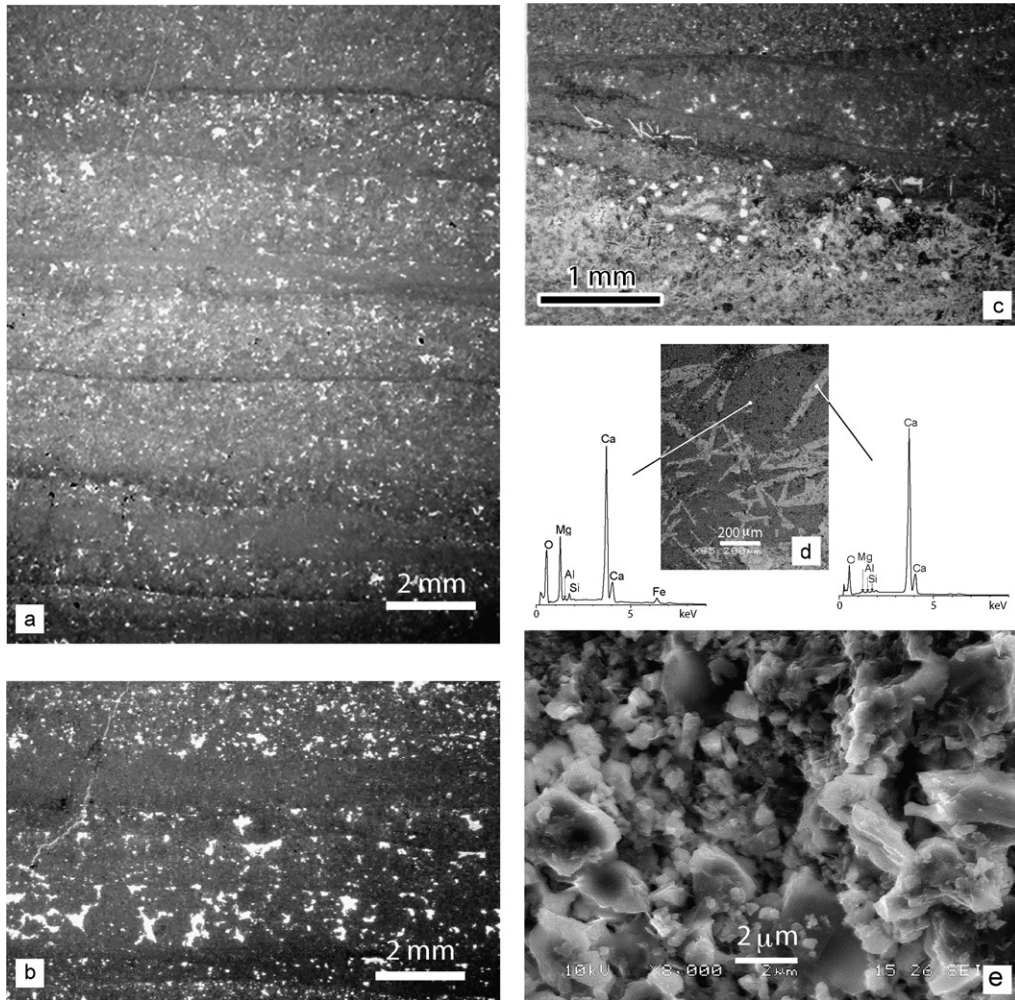


Fig. 3. (a) Successive sedimentary sequences in dolostone 7115 (microfacies A). (b) Detail of birdeye or fenestral fabric in dolostone 7146. (c) Peloidal layers topped by subparallel to onlapping microbial mats in dolostone 7122; notice the fibrous evaporitic pseudomorphs. (d) BSE image of evaporitic pseudomorphs in dolostone 7149, with EDS analyses of pseudomorph and dolomicrite. (e) SEM image of dolomicrite (7114).

Fig. 3. (a) Séquences sédimentaires successives dans la dolomie 7115 (microfacies A). (b) Détail de la fabrique fenestrée (avec *bird eyes*) dans la dolomie 7146. (c) Lamines pelloïdales surmontées de films microbiens subparallèles ou à angle faible dans la dolomie 7122; on remarque des pseudomorphes évaporitiques fibreux. (d) Image en électrons rétrodiffusés des pseudomorphes évaporitiques de la dolomie 7149, avec analyses EDS. (e) Image MEB de la dolomicrite de l'échantillon 7114.

Fenestrae (Fig. 3b) suggest the temporal development of a microbial mat limiting gas outflow from the sediment. This is supported by the recognition of typical microbial laminae located at the top of the peloidal dolostones (samples 7112, 7122, and 7146). These crinkled microbial mats show parallel, or sometimes low-angle and onlapping, laminae, and generally follow the substrate micromorphology, suggesting that the substrate was temporarily exposed to quiet water conditions. The microbial colonization phases stabilized the sediment. These features are evidence of deposition in a stable, protected mud flat

environment. Locally, aggregates of randomly interlocked pseudomorphs after gypsum crystals, fibrous to lozenge-shaped and up to 1 mm long, grown upwards from the bottom of a lamina, are replaced by mosaics of microsparitic calcite (Fig. 3c and d). The crystal habit of the pseudomorphs is common in evaporitic deposits, and is usually interpreted as a result of either early-diagenetic interstitial precipitation from hypersaline pore-fluids or intrasedimentary growth in the phreatic or capillary zones [3].

- The upper part (sample 7149) is characterized by thinner laminae. Each lamina is limited upwards by a

wavy microbial structure of stromatolitic aspect, consistent with the lack of long emersions.

All these sedimentary features are typical of peritidal environments (i.e. the temporarily emerged subtidal, intertidal and sometimes aerially exposed supratidal zones), analogous to present littoral lagoons or sabkhas formed under warm semi-arid conditions, such as can be observed along the Persian Gulf [35]. The temporal evolution is marked by the development of more protected conditions. The quality of preservation of the microstructures is such that the dolomicrite precipitation must have been penecontemporaneous with sedimentation. Bird eyes and laminoid fenestrae are interpreted as the consequence of release of fluids due to organic decay, mainly microbial in origin, whereas submillimetre-scale vugs represent early-diagenetic dissolution processes.

By contrast, the limestones up section display larger sparitic crystals formed during secondary recrystallization. Primary sedimentary features are hardly recognizable, although variations in crystal size sometimes mimic ghost laminae or microbial mats.

3.2. Mineralogy

In order to determine their mineralogy, a few samples were selected for X-ray analyses and mapping of selected areas was carried out using the electron microprobe. The lower dolostones (7102 and 7109) contain dolomite with silicate minerals and subordinate calcite. Clastic quartz and K-feldspar grains are cemented by or embedded in dolomite, but they display a narrow calcite coverage (5 μm in thickness; Fig. 2g). Kaolinite or illite is sometimes present in the pore space. Irregular fillings (50–200 μm thick) of goethite are detected locally and regarded as late minerals. The intermediate dolostones (7115, 7122, 7146) contain predominantly dolomite, and less than 3% calcite. Silicate minerals are rare (<5%) and mostly consist of kaolinite or illite, 5–10 μm in size, filling interstices. The uppermost limestones (7154) contain only one carbonate mineral, which is calcite.

Cathodoluminescence microscopy of selected thin sections yielded a dominant red luminescence, which is ascribed to a Mn-rich dolomicrite ([36]; Fig. 2h). Carbonate coatings on lithoclasts and microstalactites grown from the top of small cavities in the lower dolostones display the same red luminescence suggesting also Mn-enrichment, hence confirming that they are nearly coeval with the micritic cement. A yellowish luminescence ascribed to a later Mn-poor calcite appears in some microfractures.

Scanning electron microscopy (SEM) images show that the dolomicrite contains crystals in the 1- to 5- μm (mainly 1–3) size range (Fig. 3e). A backscattered electron (BSE) image from the elongate pseudomorphs clearly shows that these crystals are polycrystalline. EDS analyses (Fig. 3d) confirm their purely calcitic composition.

4. Geochemistry

4.1. Analytical procedures

Major and trace elements as well as C and O isotopes were analysed from chemically untreated bulk samples at the SARM–CNRS laboratory in Nancy (analyst: Jean Carignan). Rock samples were ground using agate mortar. Different aliquots were used for elemental and isotopic analyses. The samples were fused with LiBO_2 and the resulting glasses were dissolved in HNO_3 . Major elements were analyzed by ICP–AES with analytical uncertainties generally less than 2%. Trace elements were analysed by ICP–MS, with analytical uncertainties generally less than 10%. Quality of the analyses was checked by comparison with international geostandards.

Carbon and oxygen isotopic compositions of carbonates and carbonate abundances have been measured by classical stable isotope techniques. The proportions of calcite and dolomite in the bedload were manometrically determined, as CO_2 released by selective reaction with > 100% H_3PO_4 [39]. Synthetic and natural standards were used to calibrate the time and the temperature of reaction necessary to separate CO_2 produced by the dissolution of calcite and dolomite. More than 99% of the calcite had reacted after 3 h at 25 °C, while dolomite contributed to less than 5% of the produced CO_2 . The remaining carbonate was then reacted for > 100 h at 50 °C. $\delta^{18}\text{O}$ (SMOW) and $\delta^{13}\text{C}$ (PDB) were measured on released CO_2 , using a modified VG-602 mass spectrometer. Overall reproducibility is $\pm 0.1\text{‰}$ for $\delta^{18}\text{O}$ and $\delta^{13}\text{C}$.

Sr isotopes were analysed at LMTG (Toulouse). The samples were first leached with cold suprapure 80% acetic acid during 24 h to remove contaminant strontium related to clay minerals. Then, the samples were partially dissolved in suprapure 80% acetic acid at 90 °C for 24 h. The solution product was evaporated, redissolved in HNO_3 (2 N), centrifuged and ‘eluted’ in Sr-SPEC columns. Sr isotope ratios were determined by TIMS. Quality of the analyses was checked by comparison with two standards: NBS 987 standard (theoretical value: 0.71025; measured value:

Table 2
Elemental and isotopic compositions of the Bwipe cap carbonates

Tableau 2
Composition élémentaire et isotopique des *cap carbonates* de Bwipe

	Dolostones												Limestones										
Samples	7099	7102	7104	7106	7109	7112	7114	7115	7119	7122	7129	7134	7136	7140	7142	7144	7146	7147	7149	7150	7151	7152	7154
SiO ₂ (%)	3.00	5.84	3.20	3.64	5.02	4.85	3.8	3.41	3.81	3.41	3.82	3.60	3.57	3.72	3.87	3.42	2.47	2.86	3.81	5.05	10.31	13.49	3.69
Al ₂ O ₃	1.11	1.75	1.15	1.37	1.29	1.29	1.34	1.22	1.30	1.15	1.37	1.38	1.26	1.36	1.35	1.24	1.04	0.93	1.45	1.18	2.37	3.4	1.07
Fe ₂ O ₃ ^a	1.04	1.36	0.77	0.93	1.14	1.06	0.98	0.92	1.00	1.21	1.28	1.24	1.35	1.39	1.01	0.73	0.64	0.88	1.44	0.81	1.21	1.99	0.57
MnO	0.15	0.16	0.10	0.10	0.19	0.09	0.09	0.1	0.1	0.14	0.13	0.14	0.12	0.13	0.11	0.09	0.07	0.13	0.16	0.16	0.16	0.12	0.12
MgO	18.26	14.28	18.52	18.02	17.59	17.80	17.76	18.42	17.64	18.4	17.63	17.68	17.5	17.46	17.8	17.98	18.48	19.36	17.98	13.35	3.66	1.61	0.43
CaO	31.46	33.94	30.65	31.38	30.24	30.63	31.19	30.56	31.03	30.68	31.06	31.07	31.25	31.28	31.46	31.6	31.13	30.29	30.7	35.85	43.39	42.69	52.74
Na ₂ O	0.05	< dl	< dl	0.12	< dl	< dl	0.12	0.12	0.13	0.11	0.13	0.11	0.09	0.15	0.08	0.07	< dl	< dl	0.09	< dl	< dl	< dl	< dl
K ₂ O	0.09	0.20	0.16	0.19	0.19	0.18	0.19	0.15	0.2	0.15	0.19	0.18	0.17	0.16	0.18	0.17	0.07	0.05	0.14	0.11	0.36	0.53	0.13
TiO ₂	< dl	0.05	< dl	0.05	0.05	< dl	0.05	0.05	0.05	< dl	< dl	< dl	< dl	< dl	< dl	< dl	< dl	< dl	0.07	< L.D.	0.08	0.09	< dl
P ₂ O ₅	0.08	0.07	< L.D.	0.1	< L.D.	0.09	0.05	0.06	0.06	0.08	0.07	0.1	0.08	0.09	0.06	0.07	0.1	0.1	0.07	0.07	< dl	< dl	< dl
I.i.	44.24	41.74	44.25	43.93	43.04	43.25	43.62	44.32	43.81	44.13	43.91	43.56	43.78	43.63	43.63	44.31	45.12	44.87	44.12	42.87	38.43	35.84	41.39
Total	99.48	99.39	98.8	99.83	98.75	99.24	99.19	99.33	99.13	99.46	99.59	99.06	99.17	99.37	99.55	99.67999	99.12	99.47	100.03	99.45	99.97	99.75999	100.14
As (ppm)	7.7	12.0	2.4	1.4	6.9	4.5	2.3	1.7	1.1	4.2	0.5	< dl	< dl	< dl	0.5	1.8	1.0	2.1	3.6	2.0	1.2	1.3	0.6
Ba	168	294	120	65	202	141	87	61	59	93	48	63	46	54	65	128	68	42	92	681	662	404	905
Cd	2.0	3.8	2.3	1.4	2.0	2.7	1.1	1.6	1.3	2.6	0.8	0.8	1.0	0.7	1.0	2.4	0.5	1.7	3.8	0.8	1.4	1.0	1.0
Cu	20	16	32	11	12	17	16	12	20	15	19	14	15	18	12	11	17	17	33	9	10	15	11
Mo	0.8	2.2	< dl	< dl	1.6	1.1	< dl	< dl	< dl	0.6	< dl	< dl	< dl	< dl	< dl	< dl	< dl	< dl	< dl	0.6	< dl	< dl	< dl
Ni	30	17	24	12	15	20	9	13	11	18	7	7	5	6	6	15	< dl	6	22	7	12	21	< dl
Rb	5	8	7	8	7	8	8	7	9	7	9	9	9	8	8	7	6	5	7	7	15	21	8
Sr	74	59	58	56	67	57	57	63	53	66	50	50	55	53	51	57	66	36	54	103	69	48	69
V	6	13	6	8	8	7	9	7	8	7	8	8	7	8	8	7	6	5	7	10	14	22	14
Zn	51	120	68	49	43	70	39	43	41	79	22	22	21	27	27	75	19	47	108	21	24	37	9
La	4.36	6.54	3.76	4.20	4.39	5.33	4.89	3.68	4.60	5.76	3.90	3.62	3.85	4.27	4.64	4.77	3.14	3.59	10.08	3.85	7.84	12.21	6.02
Ce	8.79	11.48	6.71	7.21	9.19	8.55	8.29	6.70	7.83	9.84	6.84	6.68	6.98	6.82	7.80	8.01	5.33	5.14	14.86	9.85	18.50	20.13	12.07
Pr	1.03	1.60	0.95	0.97	1.20	1.25	1.19	0.94	1.11	1.48	0.91	0.89	1.00	1.03	1.19	1.16	0.77	0.81	2.30	1.26	2.36	2.76	1.54
Nd	4.18	6.64	3.82	4.38	5.03	4.74	5.05	3.65	4.27	5.96	3.43	3.63	3.75	4.28	4.53	4.58	3.02	3.19	9.14	5.46	9.80	10.30	6.04
Sm	1.07	1.55	0.86	0.86	1.26	0.99	1.06	0.80	0.92	1.33	0.68	0.60	0.78	0.83	1.02	0.98	0.72	0.62	2.04	1.21	1.78	2.02	1.29
Eu	0.32	0.34	0.20	0.20	0.30	0.26	0.30	0.19	0.25	0.32	0.16	0.14	0.19	0.22	0.23	0.24	0.15	0.16	0.52	0.30	0.49	0.50	0.35
Gd	0.94	1.31	1.05	0.80	1.18	1.15	1.09	0.88	0.91	1.40	0.64	0.68	0.72	0.83	0.93	1.02	0.62	0.71	2.41	0.91	1.64	1.66	1.00
Dy	0.94	1.17	0.83	0.75	1.04	1.22	1.03	0.72	0.94	1.43	0.70	0.52	0.60	0.78	0.82	0.96	0.54	0.60	2.33	0.84	1.22	1.39	0.83
Ho	0.21	0.24	0.17	0.18	0.20	0.21	0.21	0.13	0.18	0.31	0.12	0.09	0.12	0.17	0.18	0.24	0.13	0.14	0.48	0.14	0.27	0.28	0.17
Er	0.65	0.60	0.46	0.41	0.51	0.75	0.53	0.34	0.52	0.80	0.34	0.29	0.39	0.48	0.51	0.66	0.33	0.39	1.48	0.37	0.65	0.70	0.42
Tm	0.09	0.11	0.07	0.07	0.06	0.09	0.08	0.05	0.08	0.14	0.06	0.05	0.06	0.08	0.07	0.10	0.05	0.07	0.24	0.05	0.10	0.12	0.06
Yb	0.66	0.60	0.53	0.41	0.45	0.73	0.49	0.36	0.54	0.85	0.34	0.39	0.39	0.49	0.56	0.74	0.34	0.37	1.47	0.30	0.64	0.65	0.38
Lu	0.09	0.10	0.08	0.07	0.06	0.11	0.08	0.04	0.08	0.14	0.06	0.05	0.06	0.07	0.09	0.11	0.06	0.05	0.24	0.05	0.10	0.10	0.06
Eu/Eu ^a	1.50	1.12	0.99	1.14	1.16	1.15	1.31	1.07	1.29	1.10	1.14	1.03	1.19	1.25	1.11	1.13	1.06	1.14	1.10	1.36	1.36	1.28	1.46
Ce anomaly after[10]	-0.02	-0.08	-0.08	-0.08	-0.02	-0.12	-0.10	-0.05	-0.09	-0.10	-0.08	-0.06	-0.08	-0.12	-0.11	-0.55	-0.10	0.16	-0.15	-0.42	-0.57	-0.60	-0.81
δ ¹³ C _{PDB} (‰)	-3.34	-3.43	-3.52	-3.75		-3.48	-3.64	-3.62	-3.92	-3.68	-4.02		-4.01	-3.86	-3.65	-3.52	-3.72	-3.81	-3.97	-5.05	-6.15	-5.58	-6.51
δ ¹⁸ O _{SMOW} (‰)	25.57	25.47	25.30	26.37		25.92	26.55	26.05	26.66	26.00	26.62		26.85	27.06	26.45	26.06	26.21	27.57	26.95	23.04	21.70	23.53	23.09
δ ¹⁸ O _{PDB} (‰)	-5.18	-5.27	-5.44	-4.40		-4.83	-4.22	-4.71	-4.12	-4.76	-4.16		-3.94	-3.74	-4.32	-4.70	-4.55	-3.24	-3.83	-7.63	-8.93	-7.58	-7.58
⁸⁷ Sr/ ⁸⁶ Sr	0.706704		0.706054		0.706406						0.707290					0.707129				0.708086			
(⁸⁷ Sr/ ⁸⁶ Sr) ^b					(0.711159)																(0.714348)		

^a Fe₂O₃ total iron as Fe₂O₃; I.i.: loss on ignition; dl: detection limit.

^b No leaching and complete dissolution (for comparison).

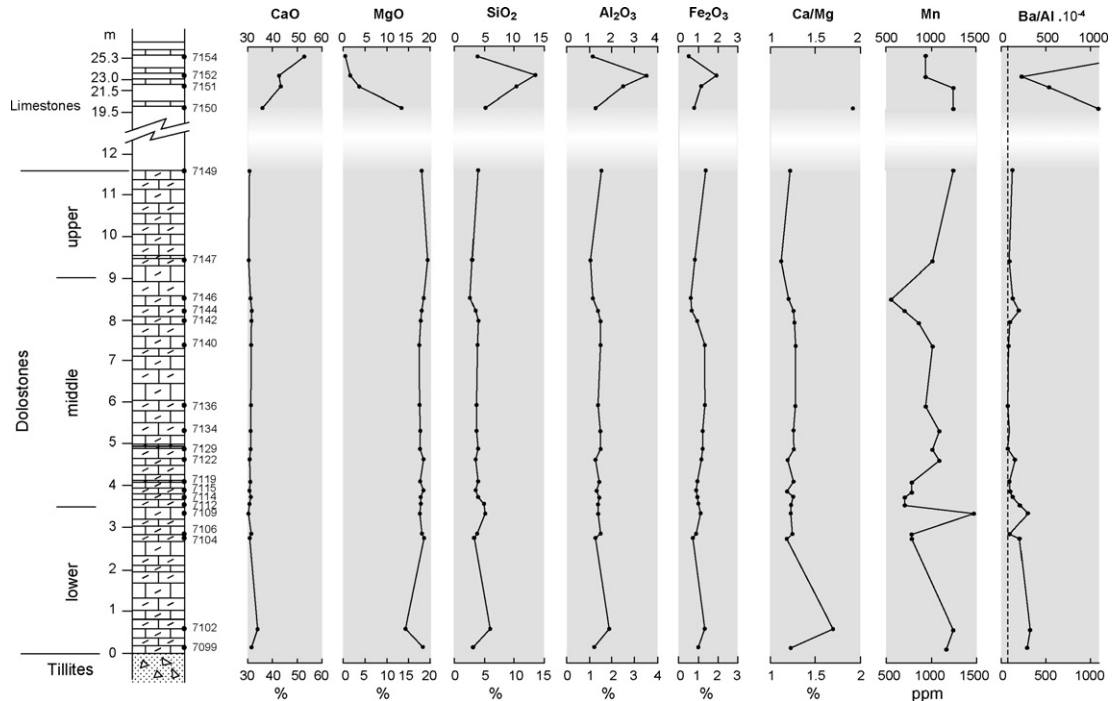


Fig. 4. Vertical distribution of major and trace elements; dashed line: Ba/Al content for average shale after [48].

Fig. 4. Distribution verticale des éléments majeurs et traces ; ligne en tiret : Ba/Al pour un shale de composition moyenne selon [48].

0.710242 ± 0.000014 at 2σ) and CAL-S calcite standard partially dissolved following the above procedure (theoretical value: 0.706924 ± 0.000018 at 2σ; measured value: 0.706934 ± 0.000013 at 2σ) standards. To check the validity of the dissolution procedure, two samples were completely dissolved without any previous leaching and analysed for comparison. Their higher Sr ratios (see Table 2) result from contamination by radiogenic ⁸⁷Sr derived from ⁸⁷Rb contained in the silicate fraction. By contrast, our partial dissolution procedure yields lower ratios reflecting the actual Sr isotope signatures of the carbonates.

Major and trace element contents and isotopic data are presented in Table 2.

4.2. Major elements

The vertical evolution of major element contents is presented in Fig. 4. Whole-rock MgO contents (14–19%) and CaO contents (30–34%) confirm that the dolostones are mainly made of dolomite or Ca-dolomite. Other constituents correspond to the previously recognized siliciclastic fragments, as confirmed by the parallel trends of SiO₂, Al₂O₃, and Fe₂O₃. The upper carbonates are more variable in compositions, with MgO contents

ranging from 13.35 to 0.43%, pointing to their variably dolomitized nature. Some limestones contain up to 20% clay minerals as evidenced by their high SiO₂ and Al₂O₃ contents (e.g., 7150).

4.3. Trace elements

Trace elements are especially important to assess palaeoenvironmental conditions and possible diagenetic effects. Their vertical evolution is presented in Figs. 4 and 5

Mn contents range from 542 to 1472 ppm in the dolostones and from 930 to 1239 ppm in the limestones. High Mn contents together with Mn/Sr > 2 are often regarded as tracers of diagenetic alteration in calcitic limestones [19], as non-marine diagenetic fluids are commonly enriched in Mn. Diagenetic alteration cannot be excluded in the Bwipe limestones, where there is evidence of secondary modifications. However, we consider the high Mn contents of the dolostones to be primary, as they roughly parallel the variations of other redox-sensitive elements. Incorporation of Mn in dolomite requires that this element is in a reduced divalent state. Yoshioka et al. [44] also interpret high Mn/Sr ratios as witnessing a peculiar seawater composition rather than diagenetic alteration.

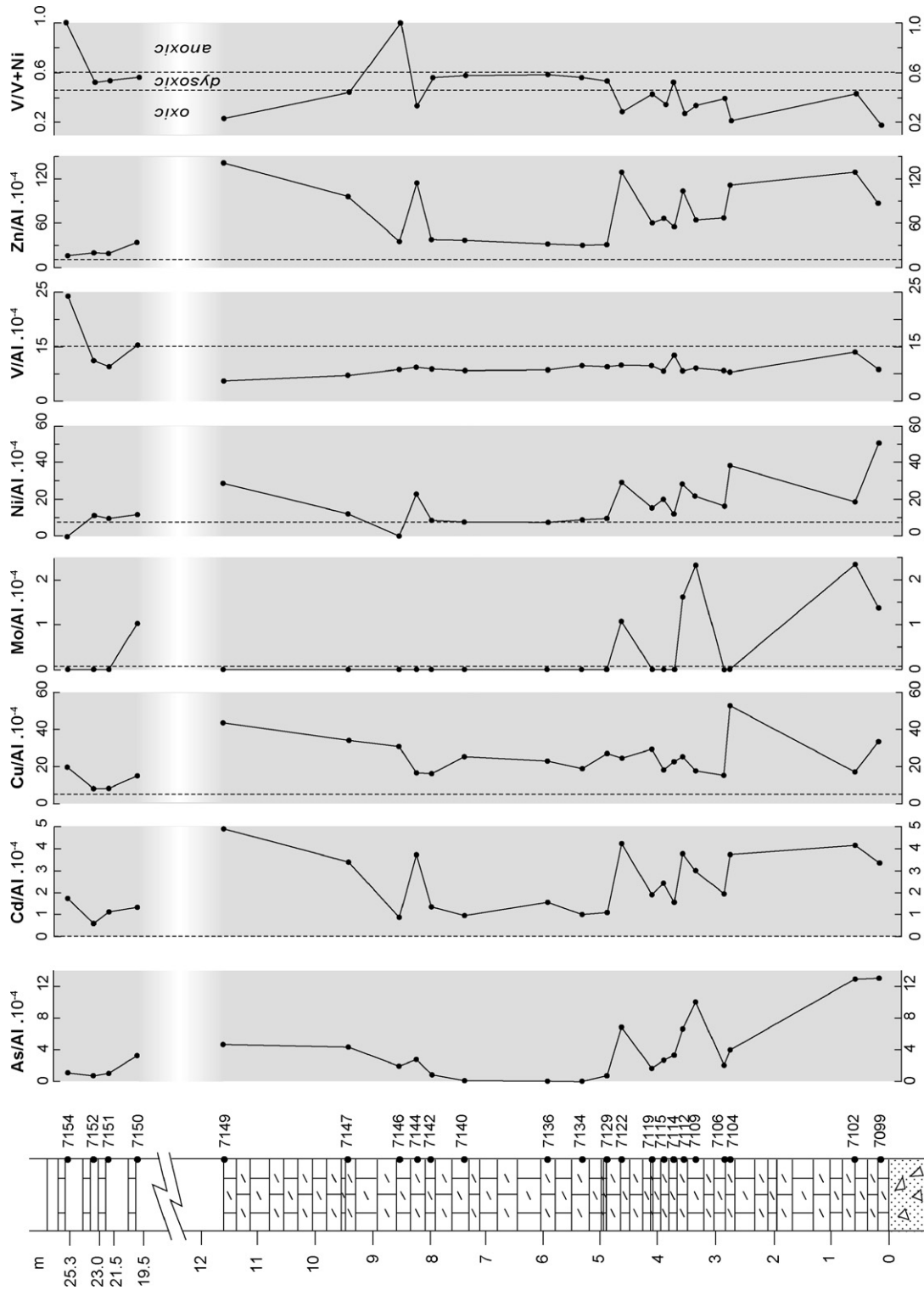


Fig. 5. Vertical distribution of Al-normalized redox-sensitive trace elements; dashed lines: Al-normalized contents for average shale after [48]; fields associated to V/(V + Ni) ratios after [37].

Fig. 5. Distribution verticale des éléments traces sensibles aux conditions rédox normalisés à Al ; tiretés : teneurs normalisées pour un shale de composition moyenne selon [48] ; domaines rédox associés aux rapports V/(V + Ni) d'après [37].

Redox-sensitive chalcophile elements such as As, Cd, Mo, Ni, V and Zn can be used to infer the redox conditions in the sediment pore water [38]. In Fig. 5, all elements are normalized to $Al \times 10^{-4}$ and compared to the corresponding average shale ratios [48] to check for a terrigenous contribution. Most values are higher than average shale ratios at specific levels in the dolostone section (especially near the base), suggesting suboxic to anoxic conditions in the sediment during these periods of time. Excess (over detrital) concentrations are either associated with organic compounds or may be derived from seawater. Cadmium is a good indicator of sulphide production from sulphate reduction [7], even at low production level. Here, its enrichment factor with respect to average shales is 40–300, suggesting that sulphate reduction was active in the sediment. V or Ni can be preferentially enriched in an organic-rich sediment column, depending on E_h , pH and sulfide activity. Thus, the $V/(V + Ni)$ ratio, or so-called

vanadium-nickel fraction, is used to precise the redox conditions in the sediment [13,27,37]. In most Bwipe dolostones, the values correspond to oxic or dysoxic conditions.

Barite formation is associated with decomposition of organic matter in pelagic sediments and Ba may even be regarded as a productivity indicator [8,9]. In nearshore areas, the relationship is not simple, but the $(Ba/Al) \times 10^{-4}$ ratio is used qualitatively in order to check excess (over detrital fraction) Ba and to look for some vertical variation (Fig. 4). The highest ratios correspond to the upper limestones. The lowermost dolomites are also characterized by relatively high Ba/Al ratios.

Total rare-earth element (REE) contents are in the typical range of marine carbonates. Moreover, the REE distribution patterns normalised to the post-Archaeon Australian shales (PAAS) often resemble the oceanic seawater distribution patterns provided by Elderfield and Greaves [11] (Fig. 6), despite a

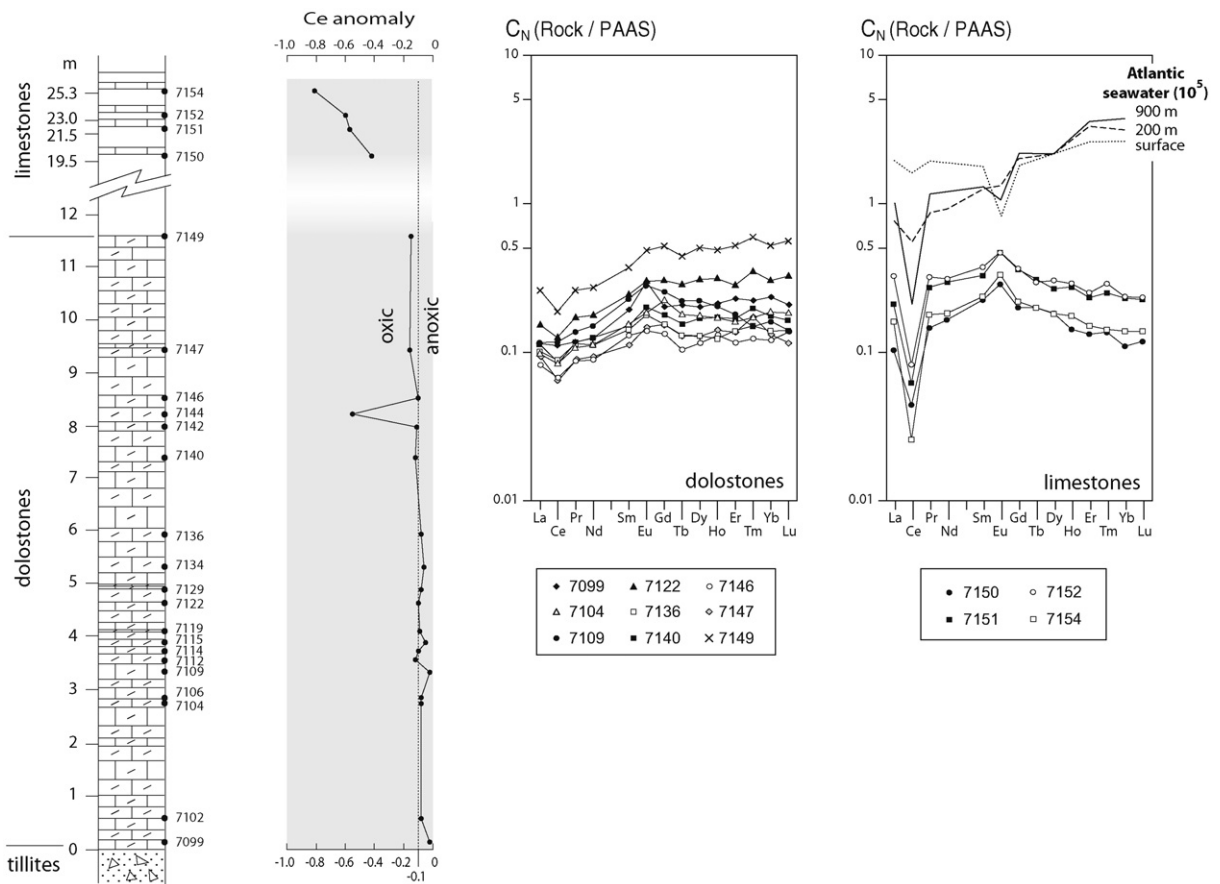


Fig. 6. Vertical distribution of Ce anomaly and rare earth element patterns normalised to post-Archaeon Australian shales (PAAS); oxic-anoxic fields after [49]; Atlantic seawater patterns (from [11]) for comparison.

Fig. 6. Distribution verticale de l'anomalie en Ce et spectres de terres rares normalisés aux shales australiens post-archéens (PAAS); domaines oxic et anoxic d'après [49]; spectres de l'eau de mer atlantique (d'après [11]) pour comparaison.

noticeable positive Eu anomaly in the Bwipe carbonates. The Ce negative anomaly of the dolostones (calculated after [10]) is small (-0.02 to -0.16), except for one sample (7144). The oxic-anoxic condition limit is at -0.1 after Wright et al. [49]. Therefore, the cap dolostones characterized by a Ce anomaly between -0.1 and -0.02 reflect anoxic or, rather, suboxic conditions in agreement with the trace metal distributions. Strongly anoxic (euxinic) conditions would yield no negative anomaly or a positive one, like in the present-day anoxic Cariaco Trench or in the Black Sea [17]. The Ce anomaly ranges from -0.42 to -0.81 in the upper limestones. In the modern ocean, values less than -0.45 are not encountered. Therefore, strongly negative values question the validity of the interpretation of the Ce anomaly as a palaeoredox proxy. Indeed, Ce depletion can also result from post-depositional alteration [40], a likely explanation in the case of the Bwipe limestones.

Trace-element contents suggest both high organic productivity and suboxic conditions in the sediment, implying that a significant number of sulphate-reducing

bacteria were likely operating at the time of sediment deposition. Nevertheless, pyrite formation did not occur, possibly because the amount of available iron was very low.

4.4. Isotopes

In the northern part of the Volta Basin, Porter et al. [34] measured $\delta^{13}\text{C}$ (‰ PDB) at -2 to -3 dropping to -8 ‰ up section. The Bwipe carbonates display a similar evolution from an average value of -3.7 ‰ in the dolostones to more negative values (-5 to -6.5 ‰) in the upper limestones (Fig. 7). Moreover, the dolostones have remarkably consistent $\delta^{13}\text{C}$ values throughout the section. These values are in the range of other Neoproterozoic cap dolostones worldwide ([15] and references therein). They are regarded as a primary basin-scale signature.

$\delta^{18}\text{O}_{\text{SMOW}}$ and $\delta^{18}\text{O}_{\text{PDB}}$ are also presented in Fig. 7. The $\delta^{18}\text{O}_{\text{PDB}}$ is around -6 ‰ in the dolostones and falls to more negative values (-9 ‰) in the limestones. Although the discrepancy between $\delta^{13}\text{C}$ and $\delta^{18}\text{O}$ values

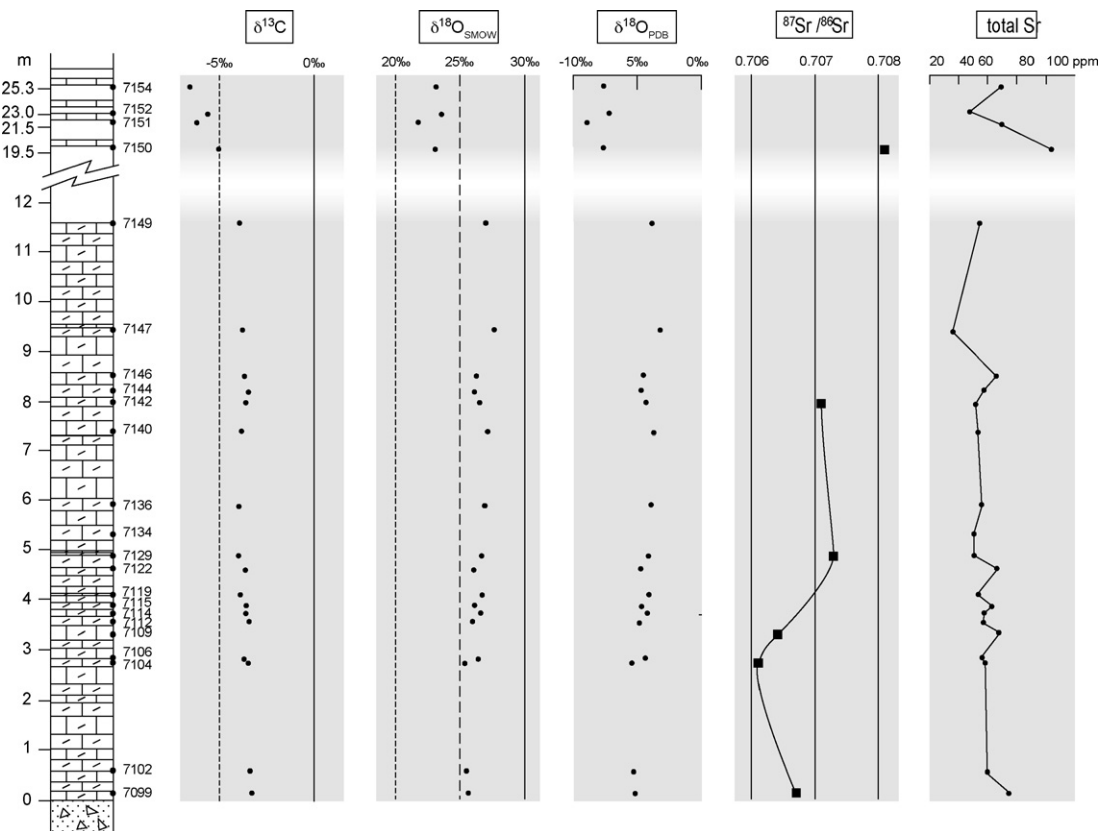


Fig. 7. Vertical distribution of isotopic compositions (C, O, Sr).

Fig. 7. Distribution verticale des compositions isotopiques (C, O et Sr).

from the dolostones and limestones are in the expected range depending upon their respective lithology [43], only the dolostone values are regarded as significant, because of their well-preserved primary sedimentological features.

Strontium contents range from 35 to 75 ppm in the dolostones and from 48 to 104 ppm in the upper limestones. $^{87}\text{Sr}/^{86}\text{Sr}$ ratios of a few samples are presented in Fig. 7. They are in the 0.7061-to-0.7073 range for the dolostones and increase in the limestones (0.7081). We consider the 0.7061–0.7073 values in the dolomites as reflecting the seawater signature at deposition time, as these rocks were formed in peritidal conditions and preserved primary sedimentary features. The higher Sr ratios of the limestones are regarded as non-significant, because these rocks were secondarily modified.

5. Discussion

5.1. Isotopic correlations

C and Sr isotopes are temptatively used for temporal correlations, despite many uncertainties regarding the Neoproterozoic reference curves, as well as the ages of the glaciations [5,30]. Only the cap dolostones values are plotted, because they are the most significant values. The C isotope signature alone is not sufficient to identify any Neoproterozoic glaciation in particular (Fig. 8). The low $^{87}\text{Sr}/^{86}\text{Sr}$ ratios exclude the possibility that the cap carbonates from the Volta Basin may be related to the 580-Ma-old Gaskiers (or Varangian) glaciation that followed the Pan-African Orogeny, but field relationships already permitted to reach this conclusion. Unfortunately, it is still impossible to decide between a post-Sturtian (730–680 Ma) or a post-Marinoan (630 Ma) deposition age. Using the values of the lowermost dolostones, a post-Sturtian age would be preferred. These low values are significant, as they imply either that the seawater signature was dominated by oceanic hydrothermal processes, hence mantle-like values, or that the continental detrital input was dominated by weathering of young and/or mantle-derived material.

5.1.1. A microbially-mediated model for the formation of the cap dolostones

Dolomite is well-known for being impossible to precipitate inorganically at normal surface conditions, even from supersaturated seawater, hence the so-called ‘dolomite problem’ [46]. In the Bwipé cap dolostones, sedimentological features point to the early formation

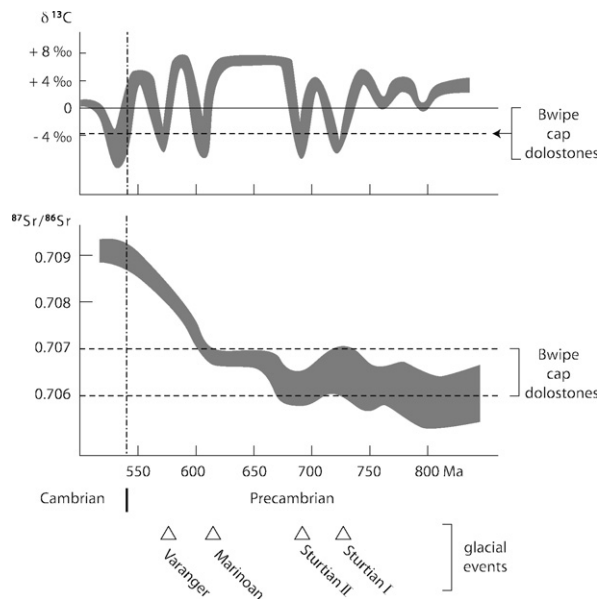
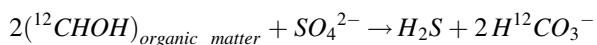


Fig. 8. Neoproterozoic seawater evolution curves for C and Sr isotopes modified after [5] and [30]; ages of glacial events after [16] and [23].

Fig. 8. Courbes d'évolution isotopique (C et Sr) de l'eau de mer néoproterozoïque d'après [5] et [29]; âges des glaciations d'après [16] et [23].

of dolomite and provide strong indications of microbial life at the time of deposition of the sediments. Trace element data are consistent with suboxic conditions developing below the sediment–water interface. Under these conditions, organic matter is degraded by sulphate-reducing bacteria yielding light-carbon-enriched bicarbonate by the reaction:



In the absence of free iron that could induce pyrite formation, H_2S is either lost in the aqueous medium or consumed by sulphur-oxidizing bacteria, often associated with sulphate-reducing bacteria in a microbial consortium [6,32]. It can also be responsible for the spontaneous reduction of manganese [33], yielding free Mn^{2+} ions easily incorporated in the precipitated carbonates. In addition, sulphate-reducing bacteria destroy the magnesium-sulphate ion pair, yielding free Mg^{2+} available for the precipitation of dolomite. Bacterially induced dolomite precipitation in anoxic conditions presently occurs in hypersaline lagoons, such as the Lagoa Vermelha (Rio de Janeiro, Brazil [42]), and has been reproduced in culture experiments [41,47]. Bicarbonate ions consumed for the precipitation of dolomite are partly derived from organic matter; hence the negative C isotope signatures of this sulphate-

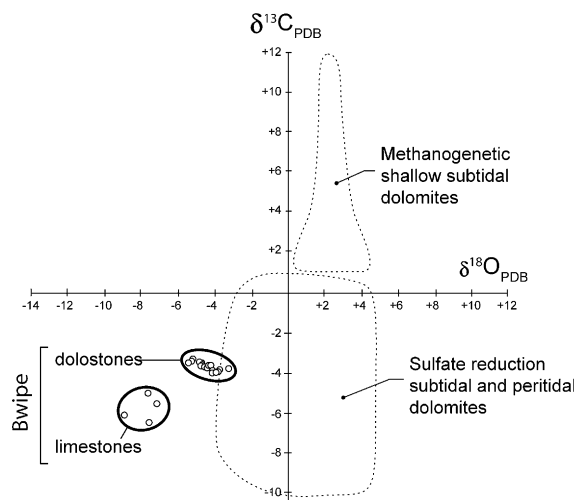


Fig. 9. Isotopic C–O diagram with fields of recent shallow marine dolostones after [29].

Fig. 9. Diagramme isotopique C–O avec domaines des dolomies marines récentes de faible profondeur d’après [29].

reduction-induced carbonate (Fig. 9). Such organogenic dolomites are not really extensive today, but they can have been more so in the shallow seas resulting from the worldwide transgression due to ice thaw in the snowball earth aftermath.

The negative C isotope signatures of cap carbonates worldwide received various explanations. The suggestion that it reflected mantle-like values due to organic productivity collapse during a Snowball ice age [14] is challenged by the undisputable ability of microbial life to survive in the most extreme environments [45]. Rather, a huge bloom of microorganic productivity is expected during the Snowball aftermath, due to warm temperatures and large inputs of nutrients provided by the reactivation of oceanic circulations and enhancement of the hydrological cycle [26]. Then, in protected environments, organic matter has been accumulating, surpassing the capacities of complete re-oxidation of the environment. In these conditions and as long as sulphate ions are available, sulphate-reducing bacteria are the dominant microbe species [28]. Despite the recognition that negative C isotope signatures witness the mediation of sulphate reducers in modern dolomites [29,42], this interpretation has not been favoured for Neoproterozoic dolomites so far. Nevertheless, intense bacterial sulphate reduction has been suggested to explain recent S isotopes data from cap carbonates elsewhere in the world [12,18]. By contrast, a lot of interest has arisen from local strongly negative C signatures regarded as the consequence of methane degassing ([22,24]). Indeed, dolomite can be formed in

the methane oxidation zone, at the boundary between the sulphate reduction zone and the methanogenesis zone [31]. In this case, highly variable, negative to strongly negative carbon isotope signatures are expected, but the relevant carbonates are local and volumetrically minor. However, sulphate-reduction and methanogenesis are generally mutually exclusive [29]. Methane-producing bacteria are strict anaerobes and can only use small organic metabolites produced by fermenters [33]. They strongly fractionate light carbon in methane, indirectly yielding ^{13}C -enriched bicarbonate, hence the positive C isotope signatures of dolomites produced in the methanogenic zone (Fig. 9). Such a positive signature is generally not observed in the cap carbonates directly overlying glaciogenic rocks worldwide. Hence, we favour the hypothesis of dolomite formation in the sulphate-reduction zone.

6. Conclusions

The Volta cap dolostones display primary sedimentary features, consistent with early precipitation of their dolomitic constituent. They were deposited just after a sharp turnover from glacial to peritidal, arid conditions in an environment dominated by microbial activity, as indicated by the abundance of microbial mats, the preservation of relict microbial filaments and geochemical proxies for high organic productivity. Redox-sensitive trace element contents imply suboxic conditions in the sediment, suggesting that organic matter was degraded by sulphate-reducing bacteria. Precipitation of dolomite with negative C isotope signatures is regarded as the consequence of this microbial activity, which destroyed the magnesium–sulphate ionic pairs and produced organic-derived ^{12}C -enriched bicarbonate. Such a microbially-mediated process was recently observed in present-day field analogues and in culture experiments. It is proposed that bacterial sulphate reduction is responsible for the specific characters of cap dolostones worldwide in the aftermath of the Neoproterozoic Snowball Earth.

Acknowledgments

Fieldwork and analytical costs were supported by the CNRS–ECLIPSE program. Technical assistance by A.C. Abraham, T. Aigouy, C. Cavaré-Hester, J.-F. Mena and F. de Parceval is acknowledged. J.-L. Bouchez (Toulouse) and M. Pagel (Orsay) are warmly thanked for the cathodoluminescence image, and O. Pokrovsky (Toulouse) for some mineral determination and many stimulating discussions. Reviews by G. Halverson,

G. Shields and N. Tribouillard helped to improve the manuscript.

References

- [1] P. Affaton, Le bassin des Volta (Afrique de l'Ouest): une marge passive, d'âge Protérozoïque supérieur tectonisée au Panafricain (600 ± 50 Ma), Collection Études et Thèses, ORSTOM, 1990, 309 p.
- [2] P. Affaton, M.A. Rahaman, R. Trompette, J. Sougy, The Dahomeyide orogen: tectonothermal evolution and relationships with the Volta Basin, in : R.D. Dallmeyer, J.P. Lécorché (Eds.), *The West African Orogens and Circum-Atlantic Correlatives*, Springer, 1991, pp. 107–122.
- [3] J.-J. Alvaro, J.-M. Rouchy, T. Bechstädt, A. Boucot, F. Boyer, F. Debrenne, E. Moreno-Eiris, A. Perejón, E. Vennin, Evaporitic constraints on the southward drifting of the western Gondwana margin during Early Cambrian times, *Palaeogeogr. Palaeoclimatol. Palaeoecol.* 160 (2000) 105–122.
- [4] K. Attoh, R.D. Dallmeyer, P. Affaton, Chronology of nappe assembly in the Pan-African Dahomeyide orogen, *Precambrian Res.* 82 (1997) 153–171.
- [5] K. Azmy, J. Veizer, A. Misi, T.F. Oliveira, A.L. Sanches, M.A. Dardenne, Dolomitization and isotope stratigraphy of the Vazante Formation, São Francisco Basin, Brazil, *Precambrian Res.* 112 (2001) 303–329.
- [6] S. Castanier, G. Le Métayer-Levrel, J.-P. Perthuisot, Ca-carbonates precipitation and limestone genesis – the microbiogeologist point of view, *Sediment. Geol.* 126 (1999) 9–23.
- [7] G. Chaillou, P. Anschutz, G. Lavaux, J. Schäfer, G. Blanc, The distribution of Mo, U, and Cd in relation to major redox species in muddy sediments of the bay of Biscay, *Mar. Chem.* 80 (2002) 41–59.
- [8] W.E. Dean, J.V. Gardner, D.Z. Piper, Inorganic geochemical indicators of glacial– interglacial changes in productivity and anoxia on the California continental margin, *Geochim. Cosmochim. Acta* 21 (1997) 4507–4518.
- [9] J. Dymond, E. Suess, M. Lyle, Barium in deep-sea sediment: a geochemical proxy for paleoproductivity, *Paleoceanography* 7 (1992) 163–182.
- [10] H. Elderfield, M.J. Greaves, Negative cerium anomalies in the rare earth element patterns of oceanic ferromanganese nodules, *Earth Planet. Sci. Lett.* 55 (1981) 163–170.
- [11] H. Elderfield, M.J. Greaves, The rare earth elements in sea water, *Nature* 296 (1982) 214–219.
- [12] P. Gorjan, M.R. Walter, R. Swart, Global Neoproterozoic (Sturtian) post-glacial sulfide-sulfur isotope anomaly recognised in Namibia, *J. Afr. Earth Sci.* 36 (2003) 89–98.
- [13] J.R. Hatch, J.S. Leventhal, Relationship between inferred redox potential of the depositional environment and geochemistry of the Upper pennsylvanian (Missourian) Stral Shale Member of the Dennis limestone, Wabaunsee County, Kansas, USA, *Chem. Geol.* 99 (1992) 65–82.
- [14] P.F. Hoffman, A.J. Kaufman, G.P. Halverson, D.P. Schrag, A Neoproterozoic snowball earth, *Science* 281 (1998) 1342–1346.
- [15] P.F. Hoffman, D.P. Schrag, The snowball Earth hypothesis: testing the limits of global change, *Terra Nova* 14 (2002) 129–155.
- [16] K.H. Hoffmann, D.J. Condon, S.A. Bowring, J.L. Crowley, U–Pb zircon date from the Neoproterozoic Ghaub Formation, Namibia: constraints on Marinoan glaciation, *Geology* 32 (2004) 817–820.
- [17] W.T. Holser, Evaluation of the application of rare earth elements to paleoceanography, *Palaeogeogr. Palaeoclimat. Palaeoecol.* 132 (1997) 309–323.
- [18] M.T. Hurtgen, M.A. Arthur, The sulfur isotopic composition of Neoproterozoic seawater sulfate: implications for a snowball Earth? *Earth Planet. Sci. Lett.* 203 (2002) 413–429.
- [19] S.B. Jacobsen, A.J. Kaufman, The Sr, C and O isotopic evolution of Neoproterozoic seawater, *Chem. Geol.* 161 (1999) 37–57.
- [20] B.M. Jahn, R. Caby, P. Monié, The oldest UHP eclogites of the world: age of UHP metamorphism, nature of protoliths and tectonic implications, *Chem. Geol.* 178 (2001) 143–158.
- [21] N. James, G.M. Narbonne, T.K. Kyser, Late Neoproterozoic cap carbonates, Mackenzie Mountains, northwestern Canada: precipitation and global glacial meltdown, *Can. J. Earth Sci.* 38 (2001) 1229–1262.
- [22] G. Jiang, M.J. Kennedy, N. Christie-Blick, Stable isotope evidence for methane seeps in Neoproterozoic postglacial cap carbonates, *Nature* 426 (2003) 822–826.
- [23] B.S. Kendall, R.A. Creaser, G.M. Ross, D. Selby, Constraints on the timing of the Marinoan 'Snowball earth' glaciation by ¹⁸⁷Re–¹⁸⁷Os dating of a Neoproterozoic, post glacial black shale in western Canada, *Earth Planet. Sci. Lett.* 222 (2004) 729–740.
- [24] M.J. Kennedy, N. Christie-Blick, L.E. Sohl, Are Proterozoic cap carbonates and isotopic excursions a record of gas hydrate destabilization following earth's coldest intervals?, *Geol. Soc. Am. Bull.* 29 (2001) 443–446.
- [25] J.L. Kirschvink, Late Proterozoic low-latitude global glaciation: the snowball Earth, in : J.W. Schopf, C. Klein (Eds.), *The Proterozoic Biosphere*, Cambridge University Press, 1992, pp. 51–52.
- [26] J.L. Kirschvink, E.J. Gaidos, L.E. Bertani, N.J. Beukes, J. Gutzmer, L.N. Maepa, L.N. Maepa, R.E. Steinberger, Paleoproterozoic Snowball Earth: extreme climatic and geochemical global change and its biological consequences, *Proc. Natl Acad. Sci. USA* 97 (2000) 1400–1405.
- [27] M.D. Lewan, Factors controlling the proportionality of vanadium to nickel in crude oils, *Geochim. Cosmochim. Acta* 48 (1984) 2231–2238.
- [28] H.G. Machel, Bacterial and thermochemical sulfate reduction in diagenetic settings – old and new insights, *Sediment. Geol.* 140 (2001) 143–175.
- [29] S.J. Mazzullo, Organogenic dolomitization in peritidal to deep-sea sediments, *J. Sediment. Res.* 70 (2000) 10–23.
- [30] V.A. Melezhik, I.M. Gorokhov, A.B. Kuznetsov, A.E. Fallick, Chemostratigraphy of Neoproterozoic carbonates: implications for blind dating, *Geology* 13 (2001) 1–11.
- [31] T.S. Moore, R.W. Murray, A.C. Kurtz, D.P. Schrag, Anaerobic methane oxidation and the formation of dolomite, *Earth Planet. Sci. Lett.* 229 (2004) 141–154.
- [32] N.F. Moreira, L.N. Walter, C. Vasconcelos, J.A. McKenzie, P.J. McCall, Role of sulfide oxidation in dolomitization: sediment and pore-water geochemistry of a modern hypersaline lagoon system, *Geology* 32 (2004) 701–704.
- [33] J. Pelmont, Bactéries et environnement – adaptations physiologiques, Presses universitaires de Grenoble, 1993, 899 p.
- [34] S.M. Porter, A.H. Knoll, P. Affaton, Chemostratigraphy of Neoproterozoic cap carbonates from the Volta Basin, West Africa, *Precambrian Res.* 130 (2004) 99–112.
- [35] B.H. Purser, Sédimentation et diagenèse des carbonates néritiques récents, tome 1, Technip, IFP, 1980, 366 p.

- [36] M. de Raféllis, M. Renard, L. Emmanuel, C. Durllet, Apport de la cathodoluminescence à la connaissance de la spéciation du manganèse dans les carbonates pélagiques, *C. R. Acad. Sci. Paris, Ser. Ila* 330 (2000) 391–398.
- [37] S.M. Rimmer, J.A. Thompson, S.A. Goodnight, T.L. Robl, Multiple controls on the preservation of organic matter in Devonian-Mississippian marine black shales: geochemical and petrographical evidence, *Palaeogeogr., Palaeoclimat., Palaeoecol.* 215 (2004) 125–154.
- [38] A. Sarkar, S. Sarangi, M. Ebihara, S.K. Bhattacharya, A.K. Ray, Carbonate geochemistry across the Eocene/Oligocene boundary of Kutch, western India: implications to oceanic O₂-poor condition and foraminiferal extinction, *Chem. Geol.* 201 (2003) 281–293.
- [39] S.M.F. Sheppard, H.P. Schwarcz, Fractionation of carbon and oxygen isotopes and magnesium between coexisting metamorphic calcite and dolomite, *Contrib. Mineral. Petrol.* 26 (1970) 161–198.
- [40] G. Shields, P. Stille, Diagenetic constraints on the use of cerium anomalies as palaeoseawater redox proxies: an isotopic and REE study of Cambrian phosphorites, *Chem. Geol.* 175 (2001) 29–48.
- [41] Y. van Lith, R. Warthmann, C. Vasconcelos, J.A. McKenzie, Sulphate-reducing bacteria induce low-temperature Ca-dolomite and high Mg-calcite formation, *Geobiology* 1 (2003) 71–79.
- [42] C. Vasconcelos, J.A. McKenzie, Microbial mediation of modern dolomites precipitation and diagenesis under anoxic conditions (Lagoa Vermelha, Rio de Janeiro, Brazil), *J. Sediment. Res.* 67 (1997) 378–390.
- [43] J. Veizer, Trace elements and isotopes in sedimentary carbonates, in : R.J. Reeder (Ed.), *Carbonates: mineralogy and chemistry*, *Rev. Mineral.* 11 (1983) 265–299.
- [44] H. Yoshioka, Y. Asahara, B. Tojo, S. Kawakami, Systematic variations in C, O and Sr isotopes and elemental concentrations in Neoproterozoic carbonates in Namibia: implications for a glacial to interglacial transition, *Precambrian Res.* 124 (2003) 69–85.
- [45] J.L. Wadham, S. Bottrell, M. Tranter, R. Raiswell, Stable isotope evidence for microbial sulphate reduction at the bed of a polythermal high Arctic glacier, *Earth Planet. Sci. Lett.* 219 (2004) 341–355.
- [46] J. Warren, Dolomite: occurrence, evolution and economically important associations, *Earth Sci. Rev.* 52 (2000) 1–81.
- [47] R. Warthmann, Y. van Lith, R. Warthmann, C. Vasconcelos, J.A. McKenzie, A.M. Karpoff, Bacterially induced dolomite precipitation in anoxic culture experiments, *Geology* 28 (2000) 1091–1094.
- [48] K.H. Wedepohl, The composition of the upper Earth's crust and the natural cycles of selected metals, in : E. Merian (Ed.), *Metals and their Compounds in the Environment*, VCH-Verlagsgesellschaft, 1991, pp. 3–17.
- [49] J. Wright, H. Schrader, W.T. Holser, Paleoredox variations in ancient oceans recorded by rare earth elements in fossil apatite, *Geochim. Cosmochim. Acta* 51 (1987) 631–644.